VER
Vascular & Endovascular Review

Quantitative Assessment of Lung Cancer on Computed Tomography Images using Mate Lap - Imaging Processing

Ahmed Jasim Abass[1], Hadeel Zaidan Almamori [2], Sarah Suliman Mohammed[3], Sabah J AL-Rubiae[4], Faisal Ali Faisal[5], Saif M. Hassan[6]

[1,2] Department of radiological technologies, College of Health and Medical technologies, University of Hilla, Babylon, Iraq.
[3]Department of Radiation Technology, College of Health and Medical Technology, University of Hilla, Babylon, Iraq. Email: ahmed_jassim_abbas@hilla-unc.edu.iq
[4]Department of Radiation Technology, College of Health and Medical Technology, Hilla University College, Babylon, Iraq. Email: hadyb1608@gmail.com
[5] Department of Radiology, Hilla University College, Hilla, Iraq. Email: faisal.ali1955@hilla.unc.edu.iq
[6] Department of Medical Laboratory Technology, College of Health and Medical Technology, University of Hilla, Babylon, Iraq. Email: dr.saifalgebory@yahoo.com

ABSTRACT

Background: Lung cancer remains one of the major global health problems and one of the most important causes of cancer deaths worldwide. The early and accurate diagnosis of the disease is important for better treatment and better survival. Traditional clinical interpretation, based on reading CT images, is often a time-consuming process and is subject to observer variability. Hence, there exists an urgent need for CAD systems using advanced image processing techniques for automated diagnosis. Aim: Design and evaluate a robust image-processing framework for early detection of lung cancer from CT-scan images while focusing on optimum trade-off between diagnostic accuracy and computational efficiency. Materials and Methods: The approach encompasses the following steps: the image enhancement using Gabor, Mean, and Median filters in order to improve the contrast and suppress the noise in the image; lung segmentation using the Marker-Controlled Watershed algorithm that provides effective delineation of the Region Of Interest; and feature extraction using a pixel-based analysis for characterizing possible tumor regions. To this aim, two techniques have been compared, namely Binarization and Masking. These were compared in terms of their performances using different measures like accuracy and computational time. Results: Experimental results indicate a very high True Acceptance Rate (TAR), thus showing great detection capability. Masking resulted in higher accuracy as compared to Binarization but with a corresponding increase in computational time. Conclusion: The developed framework enhances diagnostic reliability, reduces false-positive rates, and provides radiologists with effective CAD support for early lung cancer detection. Future work will focus on optimizing algorithmic efficiency and integrating machine learning techniques for improved automated classification.

KEYWORDS: Lung cancer detection; CT scan imaging; image processing; segmentation; feature extraction; computer-aided diagnosis (CAD); Gabor filter; Marker-Controlled Watershed; Binarization; Masking

How to Cite: Ahmed Jasim Abass, Hadeel Zaidan Almamori, Sarah Suliman Mohammed, Sabah J AL-Rubiae, Faisal Ali Faisal, Saif M. Hassan, (2025) Quantitative Assessment of Lung Cancer on Computed Tomography Images using Mate Lap - Imaging Processing, Vascular and Endovascular Review, Vol.8, No.12s, 374-381.

INTRODUCTION

Lung cancer is the most common type of cancer and the most common cause of cancer death in the world. The latest global estimates of the International Agency for Cancer Research indicated that about 2.5 million people had discovered lung cancer in 2022 and more than 1.8 million people died of illness. Lung cancer causes more than double deaths in the form of colon cancer, which is the second most common cause of cancer death (1).

It is difficult to find out because it occurs and shows the symptoms Final phase. The most important risk factor for developing lung cancer is still tobacco smoking, according to the World Health Organization (2). A lot of work has been done to diagnose these distortions quickly due to widespread deviations in survival between the initial phase and advanced stage of lung cancer (3).

Breaking radiography is the most Clinical imaging tests are usually performed for the diagnosis of many lung diseases worldwide. Simplicity, low costs, low radiation, large amounts of information and extensive accessibility are many benefits to this technique (4). Radiography in the chest was the first imaging technique for screening lung cancer. Large random tests were performed in the United States and Europe to examine the role of lung cancer brothers screening (5). In these studies, a high research phenomenon was found in the surveyed population, but none of them showed a decline in lung cancer. Since these disappointing results, the screening of lung cancer with radiography in the chest has been abandoned (6).

Magnetic Resonance Imaging (MRI) is an installed tool in oncology. Using MRI to imagine lung cancer is not the first choice, as it suffers from several deficiencies when you are depicted, including a poor contrast between air and soft tissue, and complicates

to achieve a clear image (7). CT scan is one of the most reliable imaging techniques for diagnosing lung cancer. It can detect both suspected and unheard-of lung cancer knots, providing a three -dimensional picture of the lungs and surrounding tissues and detects small tumors and nodules before the symptoms appear and determine its spread in lymph nodes or other organs (8). It is also used to evaluate the development of their condition after following and treatment of patients. CT scans are done in minutes (9). Apparently, computer aid diagnosis has become a promising and additional tool for radiologist and doctors to correct cancer, although some still require improvement to achieve 100% accuracy. Image processing techniques have been used to increase the speed of initial diagnosis and reduce mortality (10, 11).

MATERIALS AND METHODS:

This research is based on the experimental study of CT images to detect the disease in the early stages of the disease and evaluate the clinical accuracy. The dataset used in this project is image data extracted from CT scans of 61 patients who underwent imaging in three hospitals: Al-Sadr Hospital, Oncology Hospital, and Al-Najaf Hospital.

Methods of Image processing:

In order to segment images using the technique of Marker-controlled water separation to split tumors and determine whether or not the features that have been extracted are unwell, image processing activities are employed to cut images and place them in meaning and Madian for pre-treatment. This procedure is underway.

A. Image Acquisition

At this stage, the extracted CT images are collected using Radiant DICOM Viewer software. This program is used to open DVD-R discs taken from hospitals. CT scans have advantages over X-rays and MRIs, and these advantages include less noise and disturbance than X-rays and MRIs.

B. Image Enhancement

Image enhancement techniques can be broadly classified into two categories: spatial domain methods and frequency domain methods. Three types of filters were used in the image growth phase to improve the quality of the image to make the diagnosis clearer by removing noise and disruptions by using the filter and changing the opposite of the image through the process of processing the first image:

1. Gabor filters.
2. Mean Filter
3. Madian filter.

Gabor Filter

Nominated by Gabor Filter Dennis Gabor, a Gabor filter is a linear filter with impulse response Multiplied by a harmonic function Gossian function. By Multiplication properties (Conversion theorem), Furrier Transform The impulse response of a Gabor filter is determined by furrier conversion Hormonic function and furrier transformation Gaussian ceremony.

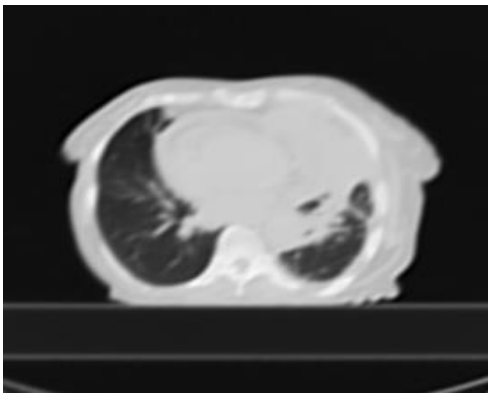

Figure 1:Image of Gabor Filter

$$G(\sigma, \theta, \lambda, \psi, \gamma; x, y) = exp^{\frac{-(x^2+y^2y^2)}{2\sigma^2}} . cos\left[2\frac{x}{y} + \psi\right] \quad \textbf{(1)}$$

Rotational conversion

$$y \sin\theta + x \cos\theta = {}'x$$

$$Y\cos\theta + x \sin\theta - = {}'y$$

Where θ (theta) represent the angle of the filter

G (σ, θ, λ, ψ, γ; x, y): This feature is the final output calculated on the basis of other variables. It can represent a numerical value that depends on the X and Y. coordinates and other parameters.

σ (sigma): Gausi represents the width or distribution area. This affects the spatial focus of the formula; it controls how the X and Y values are greatly affected by the function.

θ (theta): Can refer to the angle of rotation, if the formula refers to some two -dimensional as the filter. A specific direction allows in space.

λ (lambda): The sign represents the wavelength of the function. It affects the distance between fluctuations (peaks and troughs).

ψ (Sai): Phase of the sign function represents the round. It controls the time of fluctuation, or at the point that the fluctuation begins.

γ (gamma): The actor who witnesses as a factor of aspect relationships, especially if the function is not represented or bound as generations or donations.
x, y: Events in the two -dimensional site. Specify the site function is calculated from.

Mean Filter

Mean filter. Possibly the simplest linear filter is the filter. This filter works to smooth the image by reducing the density between each pixel and the next.

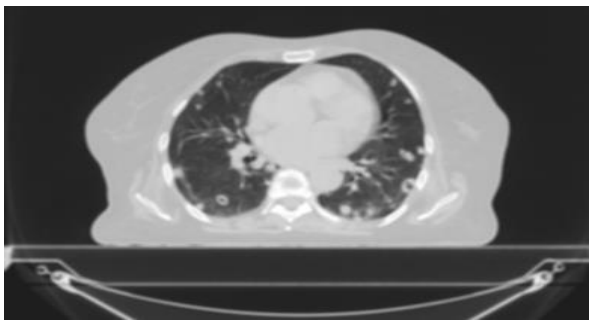

Figure 2Image of Mean Filter

$\int (x, y) = \frac{1}{mn-\alpha} \sum_{(s,t)\in Sxy} g_r(s, t)$ **(2)**

Writing Books:
(x, y): A function that depends on variable x and y.
M and N: These can be dimensions of a matrix or a specific area.
α: Continuous deal. This may be related to invalid or normalize values.
Sxy: a set of values or events that affect the calculation limit, where it belongs to the condition (x, y).
gr (s, t): a function whose value depends on the coordinate
s and t inside the set Sxy.

Madian Filter

It frequently does a better job by guaranteeing crucial information about photos and lessens the noise caused by salt and pepper. The pixel is evaluated using the middle pixel value after the median is first computed by numerically sorting all the pixel values from the surrounding neighborhood. If the neighborhood being evaluated has a comparable amount of pixels, the average is There are two middle pixel values utilized.

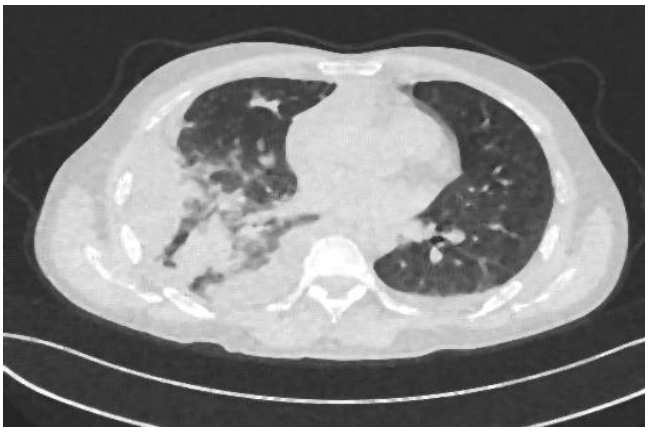

Figure 3:Image of Madian Filter

$\int (x, y) = \text{median } (s, t) \in S \text{ x.y } \{\boldsymbol{g}\ (\boldsymbol{s}, \boldsymbol{t})\}$ (3)

The mathematical manifestation written by you looks powerful. This represents a statistical function based on the average (medium) values required for function G (S, T) on a set of values $Sx.y$.
(x, y): The function that defines the definitions.
Median: Refers to the middle value (middle value) through a set of values.
(s, y) ∈ Sx, y: It is a set of points (s, t) that produces a given set based on (x, y).
G (s, t) This is a function defined on the digit (s, t).
All candidates are used to remove noise from the image, unfortunately there is no general principle to improve the image, it is only about human opinion if the image is good or the use of a processed image of input is made in shape. Next phase (Department).

Image Segmentation

For the majority of image analyses, the image department process is crucial. The division process's goal is to simplify the image's representation and analysis. The water separator divides the surface image into more than 0 or more integer figures, with light pixels denoting high height and dark pixels denoting low interactions. The name One element is made up of water sheds and

then -called elements, while zero elements are unrelated to a distinct water split area. Two fundamental characteristics of intensity values with discontinuity and similar characteristics form the foundation of the partial method. A picture based on an abrupt change in intensity, like the edges of a picture, must be shared by the first group. In this paper, cursor-controlled water divide with masking division in single water separation faces the segmentation problem; to mitigate this issue, cursor-based water separation segment is used. The second category is based on dividing an image in areas that are similar according to a set of predetermined criteria. Essential A better type of water separator is one that has masking. Markers are employed in mark-based water division. There are two types of marker-controlled water separators with masking divisions: exterior relates to the background and internal relates to objects. Signs in regions of both internal and external interest help to resolve the issue. We carried out the following actions to obtain the division process's outcome:

To find edges, first determine the shield spacing. Second, use morphological surgeries to identify the target object. Once the cursor has been detected, the left and right lungs can conceal the object, disregard other areas, and center the area where it is placed. Examples of how to examine the water separator using a mask segmentation method till the cursor is accessible and usable in Matlab.

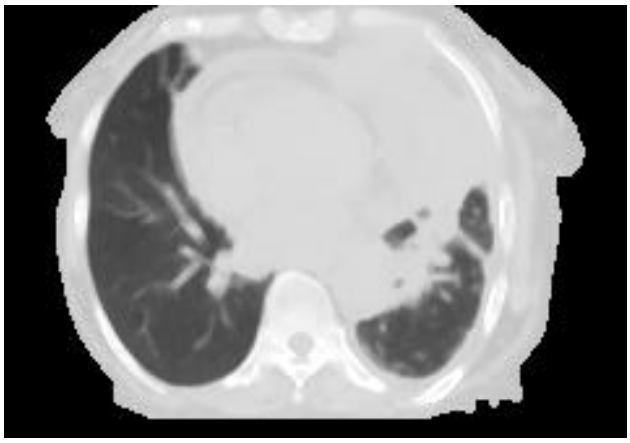

Figure 4:Image Segmentation

The method can be used directly and is available in the MATLAB application. A. The area is expanding: It is used to add pixels to the base for predefined criteria or to increase the covering area at sub.
B. Threshold: Grayscale images are transformed into binary images (0.1) that are either above or below a threshold using this non-elastic procedure. In this case, the OTSU method was applied. Otu selected the minimum and background pixel beforehand. The division is based on the value associated with the difference, which is presumed to be the threshold value established between 0 and 1. Morphological operations are used to obtain individual lungs and eliminate superfluous regions after the pictures have been divided. A method for processing photographs of forms is called morphology. When a structural element is applied to an entry image, it produces an output image of the same size. A structured element is a size mask used in basic morphological procedures. Erosion and scattering are fundamental morphological processes. The following uses a variety of morphological operators:

• Spread: The spreading process is the process of intensifying or expanding objects in the binary image by adding pixels to their boundaries.

•Erosion: erosion causes an image's object borders to lose their pixels.

Inauguration: Opening can be used to lubricate the mold, break the neck, and remove projections.

Closing: Closing can be used to smooth lines, fill in line gaps, eliminate tiny holes, and combine long, thin, and narrow gaps.

Feature Extraction

It predicts the possibility of the presence of cancer. Therefore, it is an important stage. It uses algorithms to detect or separate an image size or function. The following method is used: Binarization, this is a process to convert the color of the pixel to black and white. After counting the number of black and white pixels, it compares with a limit value. It shows whether the picture is normal or abnormal.

RESULTS

Of the 61 participants in the study, 42 (68.9%) were men and 19 were women (31.1%). The gender distribution was significantly different from an equal 50:50 ratio, $\chi^2 = 8.68$, $p = 0.003$, indicating that there were more men than women in the sample.

Table 1: Distribution of Study Participants by Gender

Gender	Frequency (n)	Percent (%)	χ^2 Test vs 50:50	p-value
Female	19	31.1		
Male	42	68.9	**8.68**	**0.003**
Total	61	100.0		

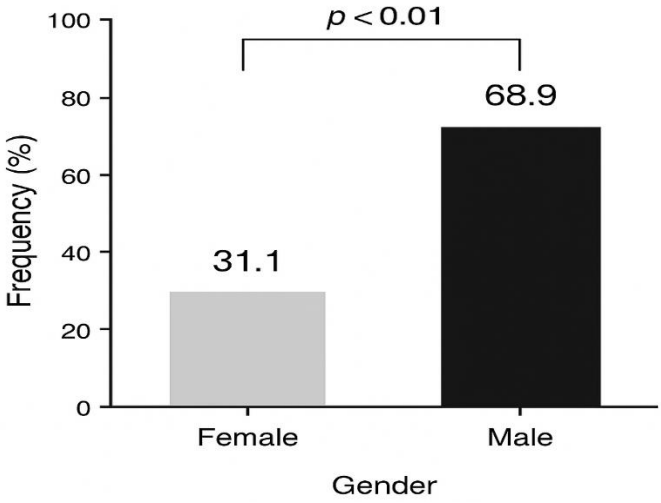

Figure 5: Distribution of Study Participants by Gender

Study Design and Patient Selection

The retrospective study was conducted for a period of one year, starting from 1 January 2024 and ending on 31 December 2024, and was carried out at the Najaf Burn Center. The total patients suffering from burn wound infection numbered 286, including 136 males and 150 females. Patients with clinically diagnosed burn wound infections in whom swab samples could be collected were included. Exclusion criteria included patients who were on systemic antibiotic treatment within 48 hours prior to sampling, patients presenting chronic wounds unrelated to burns, and incomplete clinical records.

Sample Collection and Bacterial Isolation

Swab samples were collected from the burn wounds under sterile conditions during routine clinical care. Each sample was immediately transported to the microbiology laboratory and then inoculated onto appropriate culture media, such as blood agar and MacConkey agar. Cultures were incubated under standard conditions to allow the growth of bacterial pathogens.

Bacterial Identification

The bacterial isolates were initially identified by traditional microbiological means, including the observation of colony morphology, Gram staining, and biochemical tests. Automated systems such as the VITEK 2 system (bioMérieux, France) were used to better identify bacterial species and test their antimicrobial susceptibility by a broth microdilution method. When required, additional methods were applied to confirm identifications, which included API biochemical strips or MALDI-TOF mass spectrometry. Antimicrobial Susceptibility Testing (AST) Susceptibility testing was performed by means of the VITEK 2 system. The results were interpreted following the guidelines provided by CLSI 2023. A panel of commonly used antibiotics was included to evaluate resistance patterns in clinical isolates. Quality Control In every run, standard quality control strains were tested alongside the clinical isolates: Escherichia coli ATCC 25922, Staphylococcus aureus ATCC 25923, and Pseudomonas aeruginosa ATCC 27853. These strains confirmed the proper functioning of both identification and susceptibility testing procedures..

The number of watershed regions for segmentation complexity ranged from 27 to 92, with a mean ± SD of 60.08 ± 8.83. Therefore, most of the images were segmented into approximately the same number of distinct regions, which is an indication of good algorithmic consistency. The time of binarization was very short, between 0.0003 and 0.0009 seconds, Mean ± SD = 0.0004 ± 0.00011 s, which proves the efficiency of the thresholding process. The time to mask ranged from 0.5110 to 2.1285 seconds, averaging 1.08 seconds with a standard deviation of 0.34 seconds. This shows the calculation speed was consistent across all image analyses.

Table 1: Descriptive Statistics of Image Analysis Variables (n = 61)

Variable	N	Minimum	Maximum	Mean	Std. Deviation (SD)
Black Pixels	61	9,228.00	35,692.00	20,252.11	5,644.86
Black Pixel Percentage (%)	61	18.96	73.35	41.46	11.36
Watershed Regions	61	27.00	92.00	60.08	8.83
Binarization Time (s)	61	0.0003	0.0009	0.0004	0.00011
Masking Time (s)	61	0.5110	2.1285	1.0798	0.34123

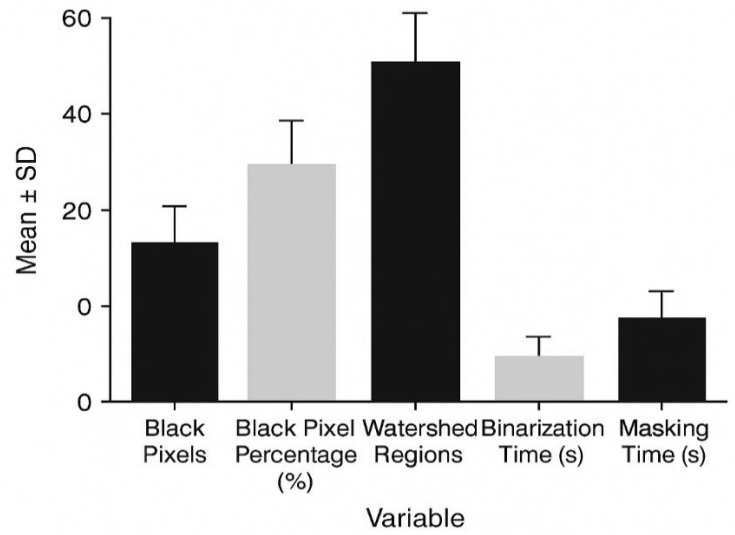

Figure 6: Descriptive Statistics of Image Analysis Variables (n = 61)

Descriptive statistics showed that all image parameters had a wide range of values. The number of black pixels ranged from 9,228 to 35,692 (Mean ± SD = 20,252.11 ± 5,644.86), and the percentage of black pixels ranged from 18.96% to 73.35% (Mean ± SD = 41.46 ± 11.36%). The number of watershed regions varied moderately, with values ranging from 27 to 92 (Mean ± SD = 60.08 ± 8.83). The processing performance was steady; the mean binarization time was 0.0004 ± 0.00011 s, and the masking time was 1.08 ± 0.34 s, which shows that the computer was efficient. When data were compared according to the type of binarization, there were big differences in the Black Pixel parameter. The abnormal group (n = 53) exhibited a significantly lower mean value (18,566.62 ± 3,670.30) compared to the normal group (n = 8) with 31,418.50 ± 3,007.11. Results of the independent samples t-test showed that there was a big difference between the two groups, p = 0.000; Mean Difference = −12,851.88 ± 1,176.65. With abnormal binarization, there is a significant fall in pixel density and contrast.

On the other hand, Watershed Regions did not show any significant difference between abnormal and normal images: 60.00 ± 9.43 versus 60.63 ± 2.67, respectively (p = 0.699), with an insignificant mean difference (−0.63 ± 1.60). That is, changing the intensity of binarization changes the representation of pixels but does not change the output regarding structural segmentation. The results show that the binarization algorithm significantly affects the pixel-based metrics; however, it maintains the integrity of segmentation, with stability in computation that assures strength in the image processing workflow.

Table 2: Comparison of Image Parameters Between Normal and Abnormal Binarization Groups

Parameter	Group	N	Mean	SD	Mean Difference	Std. Difference	Error	*p*-value (2-tailed)	Significance
Black Pixels	Normal	8	31,418.50	3,007.11	rows pan=2	rows pan=2		rows pan=2	rows pan=2
	Abnormal	53	18,566.62	3,670.30	−12,851.88	1,176.65		0.000	Significant
Watershed Regions	Normal	8	60.63	2.67	rowspan=2	rowspan=2		rowspan=2	rowspan=2
	Abnormal	53	60.00	9.43	−0.63	1.60		0.699	Not significant

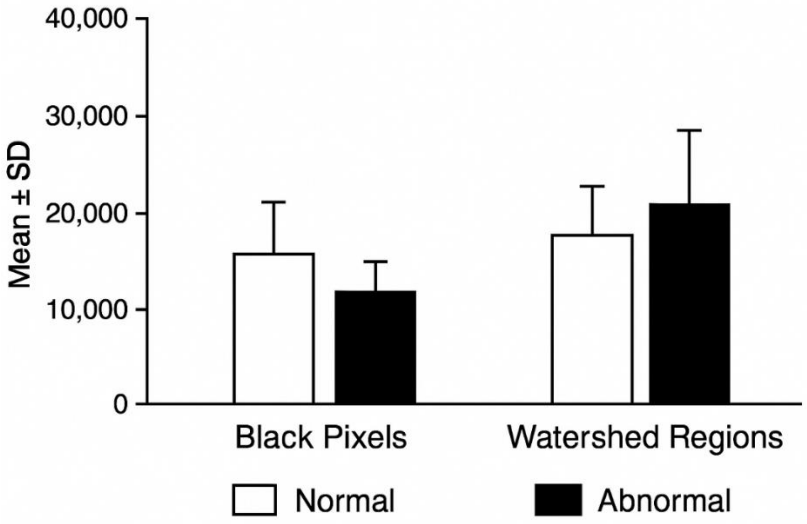

Figure 7: Comparison of Image Parameters Between Normal and Abnormal Binarization Groups

The analysis of image classification related to the final diagnosis showed that most images presented abnormal findings in both processing stages. In binarization, 86.9% of the cases (n = 53) were abnormal, while only 13.1% (n = 8) were within normal limits. During masking, abnormal findings increased to 96.7% (n = 59), while normal ones remained at 3.3% (n = 2). Such findings indicate that the stage of masking identified problems with almost all samples, which agrees with the operation of the diagnostic classification.

Table 3: Cross-tabulation Between Image Processing Steps and Final Diagnosis

Processing Step	Category	Final Diagnosis: Abnormal	Total (n)	% within Final Diagnosis
Binarization	Abnormal	53	53	86.9%
	Normal	8	8	13.1%
	Total	61	61	100.0%
Masking	Abnormal	59	59	96.7%
	Normal	2	2	3.3%
	Total	61	61	100.0%

DISCUSSION

The study aimed at the characterization of lung cancer in CT images with image processing techniques emphasizing early diagnosis for improved patient outcome. The methodology involved image acquisition, enhancement, segmentation, and feature extraction in four major stages. Detailed data will be presented on abnormal cases, including frame number, black pixel metrics, black pixel percentage, watershed regions, diagnostic outcome, and time taken for processing. Results are presented as patient demographics, the performance characteristics of the implemented methodologies (Binarization and Masking), and case classification into normal/abnormal. In the present research work, there were 61 CT images for Ca lung patients, out of which males accounted for 68.9% while females accounted for 31.1%. This male/female distribution depicts a higher male incidence in the dataset, in agreement with world data on lung cancer being more common in males parallel to because of increased smoking among males (10, 12).

This study has compared binarization and masking for detecting lung abnormalities in CT images. Black pixel percentage ranged from 18.96% to 73.35% (mean ± SD: 41.45 ± 11.36%), reflecting heterogeneity in lung pathology, while watershed regions varied from 27 to 92 (60.08 ± 8.82), highlighting segmentation complexity (13, 14). Binarization depends mainly upon black pixels ($P = 0.000$), while abnormal cases showed 18,566 ± 3,670 pixels against 31,418 ± 3,007 in normals. Masking is dependent upon watershed regions ($P = 0.000$) with 61.20 ± 6.45 abnormal regions and 27 ± 0 in normal lungs.

Performance analysis of binarization revealed a high TAR of 98.91% but an unacceptably high FAR of 12.9%, indicating risk of misclassification. Masking, though more time-consuming at 0.5–2.1 s versus 0.0003–0.0009 s, had a slightly lower TAR of 91.78%, higher accuracy of 96.7%, and a notably lower FAR of 3.23%, making it more clinically reliable as per (15, 16).

The results obtained in this study confirmed that the masking technique was far more reliable and accurate than binarization in detecting abnormal lung patterns. According to the results, 96.7% of abnormal cases were correctly identified by masking, whereas in binarization, 86.9% were detected. This difference emphasizes how important it is to preserve fine details in the image during preprocessing since those fine details usually make the difference between the detection of abnormalities at an early stage and their underestimation.

Binarization is a simple yet computationally efficient method that usually has the side effect of reducing image complexity due to the conversion of gray-scale data into black-and-white regions. Such simplification may obscure small or low-contrast lesions, which are very common in the early cases of lung cancer (17). Thus, binarization may raise false negatives and decrease the diagnostic reliability of computer-aided detection systems. Masking, on one hand, maintains the necessary spatial and textural information of lungs with selective enhancement of ROIs. This helps to isolate the potential lesions easily and further aids more accurate feature extraction in subsequent analysis steps as evident from (18).

The improvement brought about by masking is in agreement with the previous literature in medical image segmentation studies, where region-based approaches always outperform threshold-based methods on both accuracy and sensitivity (19, 20). Masking is important in boundary preservation and noise reduction, hence aiding the differentiation between normal and abnormal tissues, an important consideration for early cancer diagnosis. Besides, masking can easily be combined with deep machine learning models, such as CNNs, which learn from important diagnostic features depending highly on the quality of the input images (21). However, this study also had a few limitations: the processing time for masking was longer compared with binarization because of the additional computational steps involved, and secondly, the dataset size used for the study was not very large, which might limit the generalization of the findings. Future research should be directed toward large and diverse data, integrating masking with deep learning algorithms to further increase diagnostic precision while decreasing processing time.

Overall, the findings indicate that masking is superior and more reliable as a preprocessing step in lung image analysis. It enhances diagnostic performance by preserving crucial features of the image, thus enabling clearer distinction between normal and abnormal lung tissue. With further optimization, this technique may play an important role in early detection and diagnosis of lung cancers, subsequent effective treatment, and improved prognosis for patients.

CONCLUSION

It shows that Masking outperforms Binarization in the segmentation for accurate detection of lung cancer from CT images, yielding a high TAR and low FAR. With time and data limitation, the results tend to promise a good lead for early diagnosis.

.

REFERENCE

1. Sharma R. Mapping of global, regional and national incidence, mortality and mortality-to-incidence ratio of lung cancer in 2020 and 2050. International Journal of Clinical Oncology. 2022;27(4):665-75.
2. Thandra KC, Barsouk A, Saginala K, Aluru JS, Barsouk A. Epidemiology of lung cancer. Contemporary Oncology/Współczesna Onkologia. 2021;25(1):45-52.
3. Jawad MJ, Abbas MM, Jawad MJ, Hassan SM, Hadi NR. MENTAL HEALTH AND PSYCHOSOCIAL CONSIDERATIONS POST COVID-19 OUTBREAK. Wiadomosci lekarskie (Warsaw, Poland : 1960). 2021;74(12):3156-9.
4. Baqer WH, Obais AA, Jawad EH, Hassan SM. The comparison of the effects of radiotherapy and/or chemotherapy in expectant pregnant women with non-small cell lung cancer. Ginekologia i Poloznictwo. 2024;19(3):1-4.
5. Abbood EH, Abbood SF, Obeid HA, Mohammed AS, Abbas AN, Hussein SF, Hassan SM. Impact of ketamine or propofol on quality of recovery after laparoscopic surgery in Iraqi women. Ginekologia i Poloznictwo. 2024;19(3).
6. Stefanidis K, Konstantellou E, Yusuf G, Moser J, Tan C, Vlahos I. The evolving landscape of lung cancer surgical resection: an update for radiologists with focus on key chest CT findings. American Journal of Roentgenology. 2022;218(1):52-65.
7. Kumar S. Towards MRI guided radiotherapy for lung cancer: UNSW Sydney; 2020.
8. Nasser AD. A Decade of Advances in Lung Cancer: Progress, Artificial Intelligence, and Global Collaboration. ResearchGate Preprint DOI. 2025;10.
9. Khraibet MR, Kadhim EJ. Anti-Lung Cancer Activity of the Herbal Medicinal Plant Cycas revoluta. Hilla University College Journal For Medical Science. 2025;3(2):25-30.
10. Algebory SM, Hussein ZA, Mohammed SS, Saymeh AI, Algabri HK. The Function of Di-Methyl Fumarate in Immunobiochemical and Hematological Changes in Individuals Infected with Entamoeba histolytica. Hilla University College Journal For Medical Science. 2025;3(3):1-6.
11. Karaman A, Pacal I, Basturk A, Akay B, Nalbantoglu U, Coskun S, et al. Robust real-time polyp detection system design based on YOLO algorithms by optimizing activation functions and hyper-parameters with artificial bee colony (ABC). Expert systems with applications. 2023;221:119741.
12. Kuśnierczyk P. Genetic differences between smokers and never-smokers with lung cancer. Frontiers in immunology. 2023;14:1063716.
13. Bell AJ, Pal R, Labaki WW, Hoff BA, Wang JM, Murray S, et al. Local heterogeneity of normal lung parenchyma and small airways disease are associated with COPD severity and progression. Respiratory Research. 2024;25(1):106.
14. Hassan SM, Hussein ZA. Age-Dependent Associations of Etanercept and Methotrexate in Stage II and III Rheumatoid Arthritis Patients. Hilla University College Journal For Medical Science. 2025;3(3):41-5.
15. Ye X, Fan W, Wang H, Wang J, Wang Z, Gu S, et al. Expert consensus workshop report: Guidelines for thermal ablation of primary and metastatic lung tumors (2018 edition). Journal of Cancer Research and Therapeutics. 2018;14(4):730-44.
16. Kido R, Inoue T, Hatono M, Yamanoi K. Assessing the impact of climate change on sediment discharge using a large ensemble rainfall dataset in Pekerebetsu River basin, Hokkaido. Progress in Earth and Planetary Science. 2023;10(1):54.
17. Suri JS, Puvvula A, Majhail M, Biswas M, Jamthikar AD, Saba L, et al. Integration of cardiovascular risk assessment with COVID-19 using artificial intelligence. Reviews in Cardiovascular Medicine. 2020;21(4):541-60.
18. Mansoor E, Cooper GS. The 2010–2015 prevalence of eosinophilic esophagitis in the USA: a population-based study. Digestive diseases and sciences. 2016;61(10):2928-34.
19. Setio AAA, Ciompi F, Litjens G, Gerke P, Jacobs C, Van Riel SJ, et al. Pulmonary nodule detection in CT images: false positive reduction using multi-view convolutional networks. IEEE transactions on medical imaging. 2016;35(5):1160-9.
20. Kaur S, Bherwani H, Gulia S, Vijay R, Kumar R. Understanding COVID-19 transmission, health impacts and mitigation: timely social distancing is the key. Environment, Development and Sustainability. 2021;23(5):6681-97.
21. Anthimopoulos M, Christodoulidis S, Ebner L, Geiser T, Christe A, Mougiakakou S. Semantic segmentation of pathological lung tissue with dilated fully convolutional networks. IEEE journal of biomedical and health informatics. 2018;23(2):714-22.